Bubble Evolution Behaviors Induced by $CaO-Al_2O_3-SiO_2-CaF_2$ Fluxes Subjected to High Heat Input Submerged Arc Welding

Zhanjun Wang [1,2], Yuyang Liu [1,2], Ming Zhong [1,2], Zushu Li [3], Cong Wang [1,2] *

[1] Key Laboratory for Ecological Metallurgy of Multimetallic Mineral (Ministry of Education), Northeastern University, Shenyang 110819, Liaoning, China

[2] School of Metallurgy, Northeastern University, Shenyang 110819, Liaoning, China

[3] WMG, University of Warwick, Coventry, CV4 7AL, United Kingdom

* Corresponding author: wangc@smm.neu.edu.cn (C. Wang)

Tel.: +86 15702435155; Fax: +86 24 23906316

ABSTRACT

Bubble evolution behaviors have been thoroughly documented from the solidified slags detached from EH36 shipbuilding steel weld metals processed by $CaO-Al_2O_3-SiO_2-CaF_2$ fluxes. As the CaF_2 content decreases, bubble retention tendency attenuates, which is largely rendered by the disappearance of fluorite and cuspidine and the formation capacity of amorphous phases. Thermodynamic calculations show that bubbles are mostly induced by the synergistic effect of decreased amount of CaF_2(g) and increased amount of SiO(g).

KEYWORDS: Welding flux; Bubble; CaF_2; SiO; Slag detachability

Due to high metal deposition rate and welding efficiency, high heat input submerged arc welding (SAW) processes have been widely applied to manufacture micro-alloyed shipbuilding steels and offshore platforms.[1-4] During SAW, fluxes have been proven to be capable of impacting alloying element transfer behaviors *via* complex slag-metal reactions at high temperatures (>2000 °C).[5] As such, compositions of targeted fluxes need to be designed and optimized to achieve desirable physicochemical properties, which will dictate welding performances, including slag detachability, arc control, etc., and ultimately determine mechanical performances of the weld joints.[6-10]

Slag detachability is an important indicator foreboding a welding trial, which is mostly controlled by thermal expansion mismatch between the slag and the weld metal (WM), phase transformation in the slag, and slag-metal interfacial reactions.[11] Ever-increasing attempts have been exercised to establish physiochemical bonding mechanisms between the slag and the metal surface.[12, 13] Investigations performed on high heat input welding have shown that the bubbles on the surface of the slag shell could deteriorate surface smoothness of the WM and worsen slag detachability.[14] Bubbles in the solidifying slag interfere with the surface formation of the WM, producing a bead surface that hampers slag removal.[14] Furthermore, bubbles may also hinder slag-metal reactions, and consequently affect the quality of welded products that are strongly dependent on alloying element transition behaviors.[5]

In view of bubble behaviors under SAW, ambiguities still remain, particularly with regard to whether bubbles could form in SiO_2-based systems, where SiO_2 is demonstrated acting as the primary slag-forming agent and effectively improving slag detachability and

arc stability.[15] Indacochea et al.[16] considered that gaseous products were extremely hard to nucleate in FeO-MnO-SiO_2, which was reported to demonstrate high interfacial tensions. Mitra et al.[17] showed that bubbles could form in the molten SiO_2-bearing flux and facilitate the nucleation of CO induced by decarburization. On the other hand, Zhang et al.[18] confirmed that the partial pressure of CO generated in the binary CaF_2-SiO_2 fluxes was not sufficient to form bubbles, and the partial pressure of SiF_4 could generate obvious bubbles on the surface of the slag shell. However, due to the invisible and highly volatile nature of the flux during the SAW process, a clear understanding of bubble evolution behaviors and its potential impact to slag detachability have yet to be fully understood, particularly under the influence of the widely applied SiO_2-bearing flux.

When designing welding fluxes, CaO, which may greatly increase the melting point and lower the contents of deleterious S and P in the WM, is generally selected due to its highly basic nature.[12, 19, 20] Al_2O_3 has been demonstrated as a beneficial ingredient that could significantly improve slag detachability.[21] In addition, SiO_2 serves as the main source of O required during welding.[5] In order to achieve excellent low-temperature impact toughness *via* optimizing the O content in the WM at 200-500 ppm,[22] oxygen-free CaF_2 is generally used to partially substitute SiO_2 to prevent excessive transfer of O to the WM.[5] Moreover, appropriate amount of CaF_2 may lead to reasonable conductivity and viscosity values to potentially minimize WM hydrogen diffusion.[23, 24]

Therefore, for the current investigation, CaO-Al_2O_3-SiO_2-CaF_2 flux system has been designed with varied CaF_2 contents to document bubble evolution behaviors under high heat input SAW for the EH36 shipbuilding steel. Changes in chemical compositions of

bubbles, as well as variations in morphology and compositions of the slag shell after welding, were thoroughly investigated to further explore possible interactions between bubbles and fluxes/slags. Gaining an insight into bubble behaviors is essential to eliminate welding surface defects, and, to a large extent, to empower fundamental understandings towards quality manufacturing.

Table I. Chemical compositions of the base metal and the electrode (wt.%)

Sample	C	Si	Mn	Ni	Cu	Cr	Al	O
Base metal	0.18	0.31	1.32	0.03	0.090	0.027	0.046	0.0007
Electrode	0.08	0.05	1.69	0.04	0.021	0.047	0.017	0.0081

A typical low-alloy steel plate, EH36 shipbuilding steel (25 mm in thickness), was selected as the base metal, along with the mild steel electrode wire (3.2 mm in diameter). To minimize compositional variations, all base metals with a length of 30 cm used for welding operations were cut from one large steel plate and manufactured by consumable electrode from one reel. Inductively coupled plasma optical emission spectrometry (ICP-OES, Optima 8300, Perkin-Elmer, USA) was employed to analyze the metallic element content. Carbon-sulfur analyzer (CS230, LECO Corporation, USA) and oxygen-nitrogen-hydrogen analyzer (ONH836, LECO Corporation, USA) were used to determine C and O contents. Chemical compositions of the base metal and the electrode are listed in Table I.

Table II. Chemical compositions (wt.%) and calculated liquidus temperatures (°C) of employed welding fluxes

Sample	Pre-experimental composition (wt.%)					Post-experimental composition (wt.%)					Liquidus temp. (°C)
	CaO	SiO_2	Al_2O_3	CaF_2	CaO/SiO_2	CaO	SiO_2	Al_2O_3	CaF_2	CaO/SiO_2	
F-1	30.00	0	10.00	60.00	-	31.72 (±0.36)	9.59 (±0.10)	0	58.69 (±0.26)	-	1481
F-2	30.00	15.00	10.00	45.00	2.00	30.60 (±0.08)	9.77 (±0.05)	15.60 (±0.14)	44.03 (±0.25)	1.96	1333
F-3	30.00	30.00	10.00	30.00	1.00	30.31 (±0.42)	9.84 (±0.06)	30.58 (±0.14)	29.27 (±0.51)	0.99	1255
F-4	30.00	45.00	10.00	15.00	0.67	30.66 (±0.42)	9.83 (±0.15)	45.09 (±0.58)	14.42 (±0.32)	0.69	1218
F-5	30.00	60.00	10.00	0	0.50	30.37 (±0.38)	9.80 (±0.15)	59.83 (±0.23)	0	0.50	1337

All CaO-Al_2O_3-SiO_2-CaF_2 fluxes were prepared using reagent grade powders of CaO (≥98.0 wt.%), Al_2O_3 (≥99.0 wt.%), SiO_2 (≥99.0 wt.%) and CaF_2 (≥98.5 wt.%). Chemical compositions and liquidus temperatures calculated by FactSage 8.1 of the designed fluxes are provided in Table II. 1000 g uniformly mixed powders were placed in a graphite crucible, and heated to 1550 °C in an electric resistance furnace under high purity (>99.999 %) Ar atmosphere at the flow rate of 0.3 L/min. During the melting process, the crucible was capped by a graphite cover to prevent volatilization of any fluorides. After holding 1550 °C for 1 hour, the premelted fluxes were rapidly quenched by cold water, crushed, and screened into 12 to 200 mesh for subsequent welding experiment. It is worth noting that the fluxes were baked in a muffle furnace at 700 °C for 2 hours to remove potential moisture and burn off any residual graphite. Compositions of the quenched fluxes were analyzed by X-ray fluoroscopy (XRF, ZXS Priums II, Rigaku, USA), as shown in Table II, where negligible changes were observed between pre- and post-experimental values.

Each steel plate was degreased and wiped with alcohol to guarantee cleanliness prior to actual welding operation. Bead-on-plate double-wires single-pass SAW (Aotai Electric Power MZS-1000/1250, Aotai Electric, China) was automatically employed with a horizontal travel speed of 500 mm/min and a total heat input of 60.0 kJ/cm (DC-850A/32V for electrode forward, AC-625A/36V for electrode backward). The slag shell was cooled to room temperature, and was removed and stored in a sealed plastic container for further measurement. A small portion of the slag shell was crushed and ground into powders for X-ray diffraction (XRD, D8 Advance, Bruker, Germany) analysis using a Cu Kα radiation

at a voltage of 40 kV and a current of 30 mA with the 2-theta scanning range between 10° and 90° at a scanning rate of 2°/min and an increment of 0.02°.

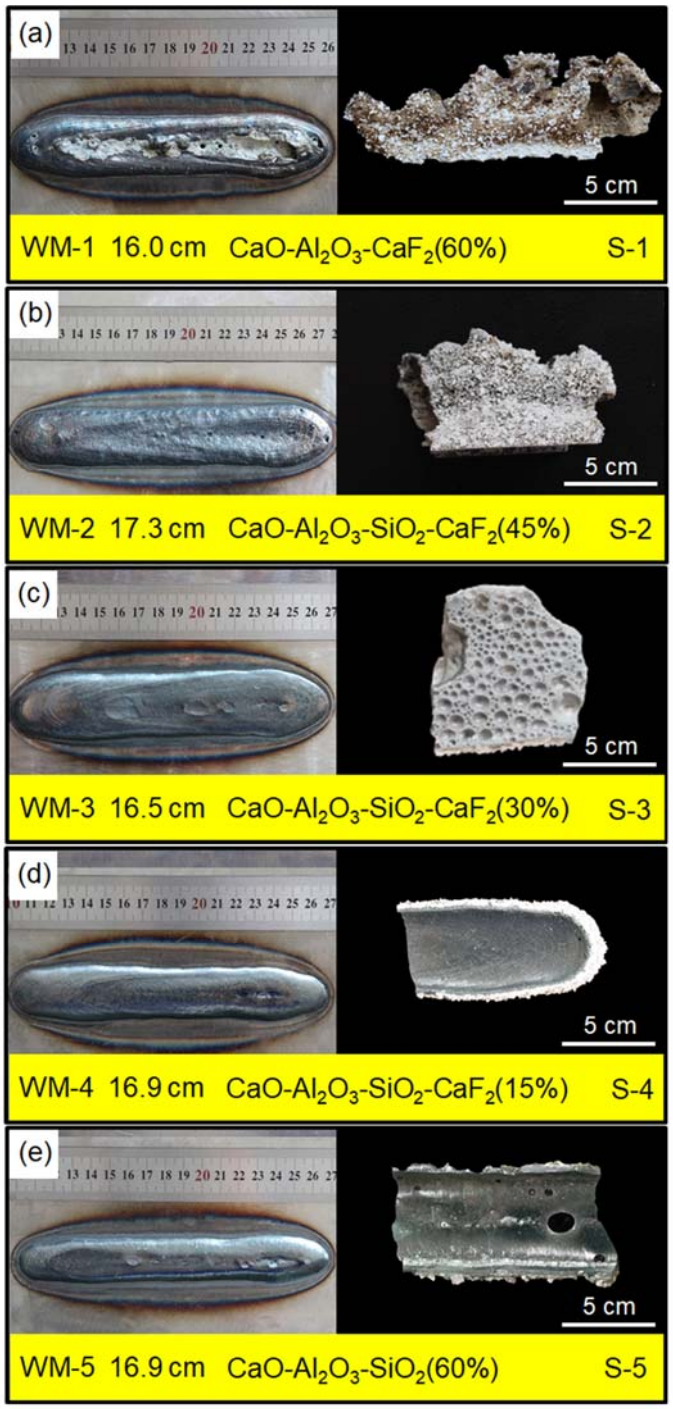

Figure 1 Macrographs of WMs and corresponding separated slag shells treated by different fluxes: (a) F-1, (b) F-2, (c) F-3, (d) F-4, and (e) F-5. (WM-1 to WM-5 are corresponding numbers of WMs

and S-1 to S-5 are corresponding numbers of slag shells)

Macrographs and effective lengths of the WMs and corresponding detached slag shells treated by the five fluxes are shown in Figure 1, where WM-1 to WM-5 are the numbers of WMs and S-1 to S-5 are the numbers of slag shells, respectively. It can be observed that the interior of the S-1 and S-2 slag shells are hollowed out by a large number of bubbles. As shown in Figure 1, WM-1 (60 wt.% CaF_2) has apparent pores and adherent slag appearing on the solidified surface. Bubbles in the slag may interfere with WM surface during solidification, resulting in the failure of the molten flux to completely cover the WM.[18] The inadequate slag removal in WM-1 may be caused by the crystalline phases with high melting points, which leads to uneven surface of the WM after welding.[25] For WM-2, the surface roughness became slightly better than that of WM-1. For WM-3, the surface becomes smoother with relatively uniform bubbles on the slag shell (S-3). It is worth noting that as the CaF_2 content in the flux decreased to 15 wt.%, the surface of WM-4 exhibits a typical fish-scale morphology while the bubbles are inconspicuous, indicating excellent slag detachability. While for WM-5, a few large bubbles appear again in the slag shell (S-5) with slightly rough WM surface. Bubbles at the slag-metal interface may lead to insufficient slag-metal reactions at the interface, thus affecting the transition of alloying elements and depreciating mechanical behaviors of the WM in later stages.[16-18, 26]

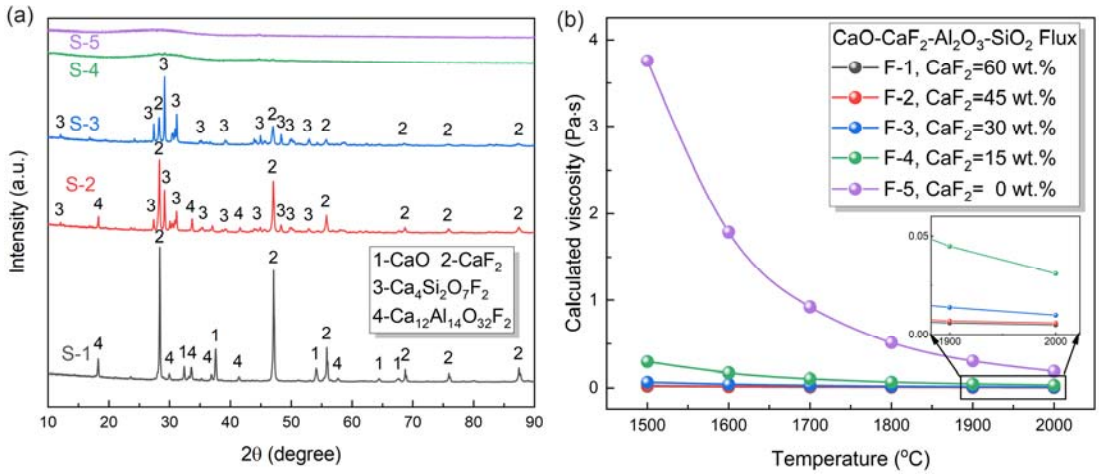

Figure 2 (a) XRD patterns of different slag shells, (b) calculated viscosity of different welding fluxes.

Figure 2 (a) shows the XRD results of slag shells subjected to different fluxes. It can be seen that for F-1, F-2 and F-3, dominant phases are found to be fluorite (CaF_2) and or cuspidine ($Ca_4Si_2O_7F_2$), which have been proven to lead to poor slag detachability.[27] Crystalline fluorite and cuspidine have high melting points,[28] and tend to prevent bubbles from escaping during the cooling process, rendering them trapped in the solidified slag shells,[29] as demonstrated in Figure 1 (a), (b) and (c). For F-4 and F-5, slag shells show unanimous amorphous behaviors, which have been accompanied by excellent slag detachability.[11] Therefore, when designing fluxes, the amorphous phase forming ability shall be taken into account in order to improve the slag detachability.

Figure 2 (b) shows the viscosity of different welding fluxes calculated by FactSage 8.1. It can be seen that, at the same temperature, the viscosity of flux S-5 is significantly higher than that of the other four fluxes. This leads to the fact that even though no crystalline phases are formed in flux S-5 (see Figure 2 (a)), bubbles may still form at the slag-metal interface, which are presumably due to the following two potential factors: a) the

adsorption force of the WM to the bubbles is greater than the buoyancy of the bubbles in the liquid slag so that bubbles are trapped at the slag-metal interface;[30] b) although the adsorption force of the WM to the bubble is smaller than the buoyancy of the bubbles in the liquid slag, the large viscosity of the liquid slag and the limited cooling time for the slag may render the bubbles impossible to float up in time and are retained at the slag-metal interface.[21, 31] Similar physical phenomena were also observed by Han and Holappa[32] that when bubbles moved to the slag-metal interface, they gradually collapsed at the interface and created a dome-like structure under the pressure of the molten slag. It should be mentioned that due to the existence of unmelted flux and sintered flux outside the slag shell and the appearance of bubbles inside and/or at the top of the slag shell, the influence of surface tension on bubble retention could be largely excluded.[33]

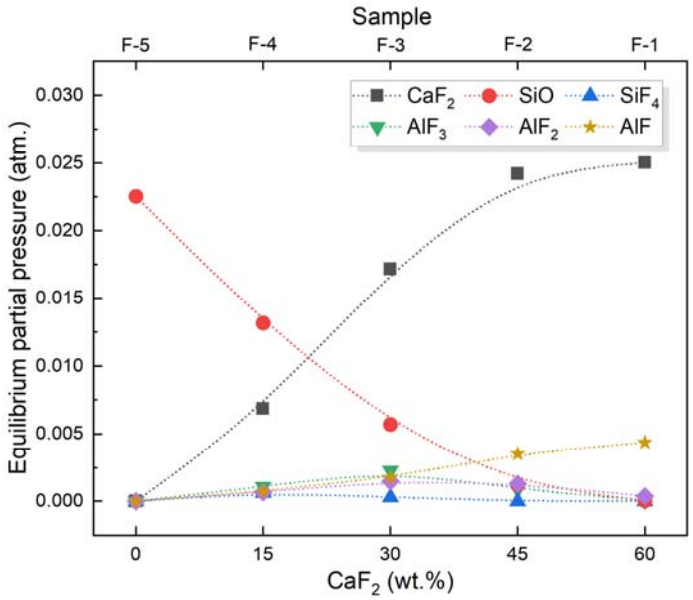

Figure 3 Equilibrium partial pressure of gases calculated by FactSage 8.1 at 2000 °C.

According to Wang et al.[15], the source of the gases generated by CaF_2-containing flux at ultra-high temperatures may be volatilized CaF_2, fluoride gases generated by reacting

with other oxides, and decomposition products of oxides under the action of plasma. Based on the gas-slag-metal equilibrium model,[18] the partial pressure of different gases at 2000 °C can be calculated by FactSage 8.1,[34] where only partial pressure values higher than 10^{-6} atm are shown in Figure 3. Detailed calculation process can be referred in the Supplemental Materials. It can be seen that the gases are dominantly composed of volatilized CaF_2(g) and SiO(g), accompanied by small amounts of SiF_4(g), AlF_3(g), AlF_2(g) and AlF(g). It is interesting to note that the amount of CaF_2(g) gradually decreases while that of SiO(g) gradually increases with lower CaF_2 content in the flux. In addition, the generated gas composition indicates that SiO_2 prefers to decompose and Al_2O_3 is more likely to react with CaF_2 to form fluoride gases at ultra-high temperature.

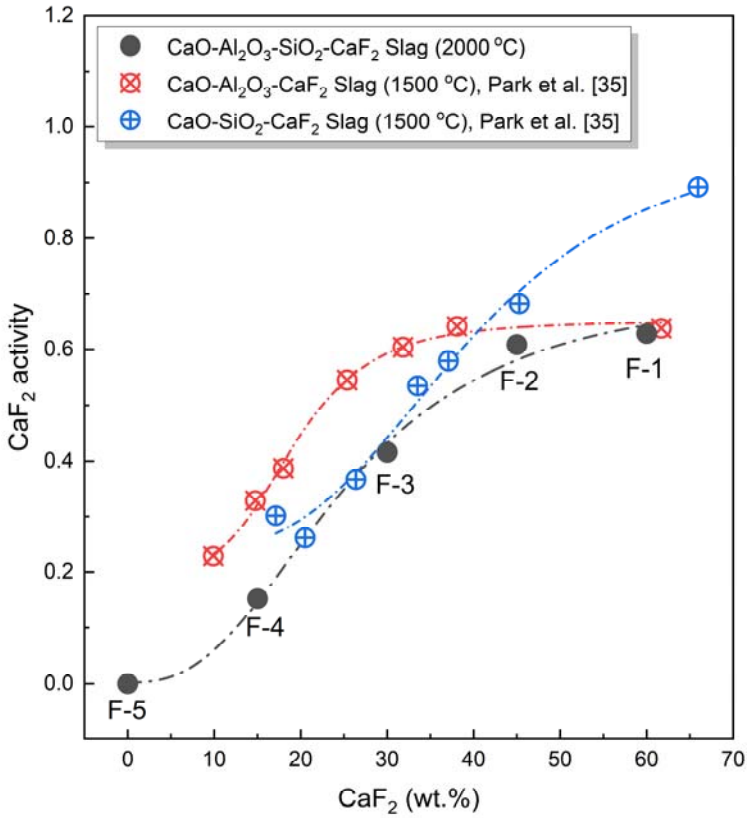

Figure 4 Activity of CaF_2 as a function of CaF_2 content in the slag.

Figure 4 shows the variation of CaF_2 activity as a function of CaF_2 content calculated by FactSage 8.1, where the activity of CaF_2 increases gradually with the increase of CaF_2 content. In the present CaO-Al_2O_3-SiO_2-CaF_2 system, the slope of CaF_2 activity reaches the maximum for the flux with an approximate CaF_2 content of 25 wt.%, and it appears to decrease with further increase of the CaF_2 content, which is consistent with the variation trends for CaF_2 activity in CaO-Al_2O_3-CaF_2[35] and CaO-SiO_2-CaF_2[35] systems. Comparing with F-3, F-4 and F-5, CaF_2 activity difference between F-1 and F-2 is negligible, which may likely be the reason for the limited partial pressure difference for the generated $CaF_2(g)$ in F-1 and F-2, as clearly shown in Figure 3. In short, when designing high heat input welding fluxes, the content of CaF_2 needs to be controlled to avoid the formation of fluorite and cuspidine with high melting points. Then, generated bubbles can escape easily from the welding flux and facilitate slag detachability. Furthermore, the characteristics of the applicable scene of the flux, including environment humidity, processing atmosphere, welding parameter, surface quality and composition of base metal, etc., should also been considered to optimize the design of the flux.[36, 37]

The present study evaluates bubble evolution behaviors in the slag shell of the EH36 shipbuilding steel treated by CaO-Al_2O_3-SiO_2-CaF_2 fluxes with varied CaF_2 contents. Main conclusions are summarized as follows:

(1) Bubbles can be generated in the molten welding flux and escape into the atmosphere, while the remainder may be trapped by the solidified slag or attached on the slag-metal interface, eventually forming pores in the slag shell.

(2) Gases generated in CaF_2-containing welding fluxes are mainly volatilized CaF_2(g) and SiO(g) decomposed by oxides. The amount of CaF_2(g) gradually decreases, while that of SiO(g) gradually increases, with the decreasing content of CaF_2 in the flux.

(3) Fluorite and cuspidine phases generated in the solidified slag shell could deteriorate slag detachability, while the slag shell composed of amorphous phases can be easily separated from the WM, resulting in excellent surface quality.

ACKNOWLEDGEMENTS

The authors sincerely thank the National Natural Science Foundation of China (Grant Nos. 52104295, U20A20277, 51861145312, 52050410341, 52011530180, 52150610494), and Research Fund for Central Universities (Grant Nos. N2025025, N2125016, N2125021).

SUPPLEMENTAL MATERIALS

The online version of this article contains Supplemental Materials, which is available to authorized users.

CONFLICT OF INTEREST

On behalf of all authors, the corresponding author states that there is no conflict of interest.

REFERENCES

1. Z. Wang, J. Zhang, M. Zhong, and C. Wang: *Metall. Mater. Trans. B*, 2022, vol. 53, pp. 1364-70.
2. J. Pu, S. Yu, and Y. Li: *J. Alloys Compd.*, 2017, vol. 692, pp. 351-58.
3. X. Li, Y. Zhang, and L. Kvidahl: *Weld. J.*, 2013, vol. 92, pp. 48-56.
4. Z. Wang, X. Zheng, M. Zhong, Z. Li, and C. Wang: *J. Non-Cryst. Solids*, 2022, vol. 591, pp. 121716.
5. J. Zhang, T. Coetsee, and C. Wang: *Metall. Mater. Trans. B*, 2020, vol. 51, pp. 16-21.

6. J.B. Kim, J.K. Choi, I.W. Han, and I. Sohn: *J. Non-Cryst. Solids*, 2016, vol. 432, pp. 218-26.
7. J.B. Kim, T.H. Lee, and I. Sohn: *Metall. Mater. Trans. A*, 2018, vol. 49, pp. 2705-20.
8. J.B. Kim and I. Sohn: *ISIJ Int.*, 2014, vol. 54, pp. 2050-58.
9. X. Xie, M. Zhong, T. Zhao, and C. Wang: *J. Iron Steel Res. Int.*, 2022, Accepted.
10. J. Sun, X. Zou, H. Matsuura, and C. Wang: *JOM*, 2018, vol. 70, pp. 946-50.
11. D.L. Olson, G. Edwards, and S. Marya: *Key Eng. Mater.*, 1992, vol. 69, pp. 253-68.
12. H. Wang, R. Qin, and G. He: *Metall. Mater. Trans. A*, 2016, vol. 47, pp. 4530-42.
13. K. Sham and S. Liu: *Weld. J.*, 2014, vol. 93, pp. 271-81.
14. B.G. Renwick and B.M. Patchett: *Weld. J.*, 1976, vol. 55, pp. 69-76.
15. C. Wang and J. Zhang: *Acta Metall. Sin.*, 2021, vol. 57, pp. 1126-40.
16. J.E. Indacochea, M. Blander, N. Christensen, and D.L. Olson: *Metall. Trans. B*, 1985, vol. 16, pp. 237-45.
17. U. Mitra and T.W. Eagar: *Metall. Trans. B*, 1991, vol. 22, pp. 83-100.
18. J. Zhang, T. Coetsee, H. Dong, and C. Wang: *Metall. Mater. Trans. B*, 2020, vol. 51B, pp. 1805-12.
19. T.W. Eager: *Weld. J.*, 1978, vol. 57, pp. 76-80.
20. T. Lau, G.C. Weatherly, and A. McLean: *Weld. J.*, 1985, vol. 64, pp. 343-47.
21. B. Singh, Z.A. Khan, and A.N. Siddiquee: *J. Mech. Eng. Res.*, 2013, vol. 5, pp. 123-27.
22. P.L. Harrison and R.A. Farrar: *J. Mater. Sci.*, 1981, vol. 16, pp. 2218-26.
23. M. Matsushita and S. Liu: *Weld. J.*, 2000, vol. 79, pp. 295-303.
24. J.E. Indacochea and D.L. Olson: *J. Mater. Energy Syst.*, 1983, vol. 5, pp. 139-48.

25. C. Natalie, D. Olson, and M. Blander: *Annu. Rev. Mater. Sci.*, 1986, vol. 16, pp. 389-413.

26. V.G. Kuzmenko: *Paton Weld. J*, 2011, vol. 5, pp. 8-12.

27. C.A. Natalie, D.L. Olson, and M. Blander: *Annu. Rev. Mater. Sci.*, 1986, vol. 16, pp. 389-413.

28. J. Yang, L. Wang, Q. Wang, J. Zhang, Y. Sasaki, C. Zhang, D. Cai, and O. Ostrovski: *Steel Res. Int.*, 2022, vol. 93, pp. 2100123.

29. Z. Duan, R. Qin, and G. He: *Metall. Mater. Trans. A*, 2014, vol. 45, pp. 843-53.

30. M. Raza, N. Kumar, and R. Raj: *Sci. Rep.*, 2016, vol. 6, pp. 1-9.

31. S. Natsui, H. Takai, T. Kumagai, T. Kikuchi, and R. Suzuki: *Mater. Trans.*, 2014, vol. 55, pp. 1707-15.

32. Z. Han and L. Holappa: *Metall. Mater. Trans. B*, 2003, vol. 34, pp. 525-32.

33. D. Obiso, D. Schwitalla, I. Korobeinikov, B. Meyer, and A. Richter: *Metall. Mater. Trans. B*, 2020, vol. 51, pp. 2843-61.

34. U. Mitra and T.W. Eagar: *Metall. Trans. B*, 1991, vol. 22, pp. 65-71.

35. J.H. Park and D.J. Min: *Steel Res. Int.*, 2004, vol. 75, pp. 807-11.

36. C.S. Chai and T.W. Eagar: *Weld. J.*, 1982, vol. 61, pp. 229-32.

37. J.H. Kiefer: *Weld. J.*, 1996, vol. 75, pp. 155-61.

FIGURE AND TABLE CAPTIONS:

Figure 1 Macrographs of WMs and corresponding separated slag shells treated by different fluxes: (a) F-1, (b) F-2, (c) F-3, (d) F-4, and (e) F-5. (WM-1 to WM-5 are the numbers of WMs and S-1 to S-5 are the numbers of slag shells)

Figure 2 (a) XRD patterns of different slag shells, (b) calculated viscosity of different welding fluxes.

Figure 3 Equilibrium partial pressure of gases calculated by FactSage 8.1 at 2000 ℃.

Figure 4 Activity of CaF_2 as a function of CaF_2 content in the slag.

Table I. Chemical compositions of the base metal and electrode (wt.%)

Table II. Chemical compositions (wt.%) and calculated liquidus temperatures (℃) of employed welding fluxes